Progress In Electromagnetics Research C, Vol. 172, 30–37, 2026
PIER C

(Received 30 March 2026, Accepted 17 June 2026, Scheduled 28 July 2026)

A Novel Subarray Division Optimization Algorithm for Sparse Arrays in Microwave Wireless Power Transmission

Jie Wang[1,2] and Jianxiong Li[1,2,*]

[1] School of Electronic and Information Engineering, Tiangong University, Tianjin, China
[2] Tianjin Key Laboratory of Optoelectronic Detection Technology and Systems, Tianjin, China

ABSTRACT: To improve beam collection efficiency (BCE) while suppressing sidelobes and limiting implementation complexity in microwave wireless power transmission (MWPT) transmitting arrays with a small number of subarrays, this paper proposes an axially symmetric sparse planar array (SDASPA) model and a one-step subarray-division algorithm named RT-DWCFPSO-SD. The proposed model exploits axial symmetry to reduce search dimension and facilitate a simplified feeding structure. The proposed algorithm jointly optimizes element positions, element excitations, and subarray boundary parameters by combining a constriction factor, dynamic inertia weight, and ring topology. Numerical simulations on an 8×8 array with an aperture of $4.5\lambda \times 4.5\lambda$ show that, when the array is divided into three subarrays, the proposed method achieves a BCE of 93.42% and a CSL of -13.19 dB. These results indicate that the proposed method is a promising design tool for MWPT transmitting arrays under limited subarray-division conditions.

1. INTRODUCTION

As a highly promising method of energy transmission, microwave wireless power transmission (MWPT) technology has demonstrated immense application potential in fields such as wireless sensor networks, drone power supply [1], medical implants [2], and space solar power stations (SSPS) since its proposal [3]. In MWPT systems, beam collection efficiency (BCE) is a key indicator for evaluating the transmitting array pattern and energy utilization efficiency within the overall system efficacy [4]. It is defined as the ratio of the power captured by the receiving aperture to the total power radiated by the transmitting antenna. Furthermore, the sidelobe level outside the receiving area (CSL) is another critical performance parameter. It affects the system's energy leakage and interference with surrounding equipment; a lower CSL implies less energy leakage and reduced electromagnetic interference to the environment, making it an important performance metric to control during design [5].

To obtain high beam collection efficiency (BCE), conventional transmitting-array synthesis methods often assign independent amplitudes and phases to all elements. However, this leads to a complicated feeding network and high implementation cost. Subarray division is therefore an effective compromise: elements with similar excitations are grouped into the same subarray, thereby reducing the number of required control channels and lowering hardware complexity [6]. Nevertheless, when the number of subarrays is small, many existing methods suffer from a noticeable degradation in BCE, which makes it difficult to satisfy MWPT requirements.

To address this issue, this paper proposes a sparsely distributed axial-symmetrical planar array (SDASPA) model and a ring-topology dynamic weight constriction factor particle swarm optimization for subarray division (RT-DWCFPSO-SD) algorithm for one-step optimization of the array layout, element excitation, and subarray division structure. Numerical simulation is used to verify the effectiveness of the proposed design framework.

Targeting the above issues, this paper proposes a novel SDASPA model and designs a one-step subarray division algorithm, named RT-DWCFPSO-SD. Unlike traditional multi-step optimization, this algorithm simultaneously optimizes element positions, excitations, and subarray structures as a unified whole. By leveraging a ring topology and introducing a constriction factor and nonlinear dynamic weights, the algorithm enhances both global and local search capabilities, enabling effective discovery of the optimal subarray division scheme within a complex solution space [7–9].

To verify the effectiveness of the proposed method, simulation experiments were conducted on a transmitting array with an aperture of $4.5\lambda \times 4.5\lambda$ and an element configuration of 8×8. The results indicate that, utilizing the proposed algorithm with dividing only 3 subarrays, the system's BCE can reach 93.42%, while the CSL is maintained at a low level of -13.19 dB. These results demonstrate that the model and algorithm proposed in this paper can maintain superior energy transmission performance while significantly reducing system cost and hardware complexity, possessing important engineering application value.

2. MATHEMATICAL MODELS OF SDASPA AND SUBARRAY DIVISION

2.1. Mathematical Models of the SDASPA and BCE

Figure 1 presents the schematic of the SDASPA model proposed in this paper. The figure displays the arrangement of

* Corresponding author: Jianxiong Li (lijianxiong@tiangong.edu.cn).

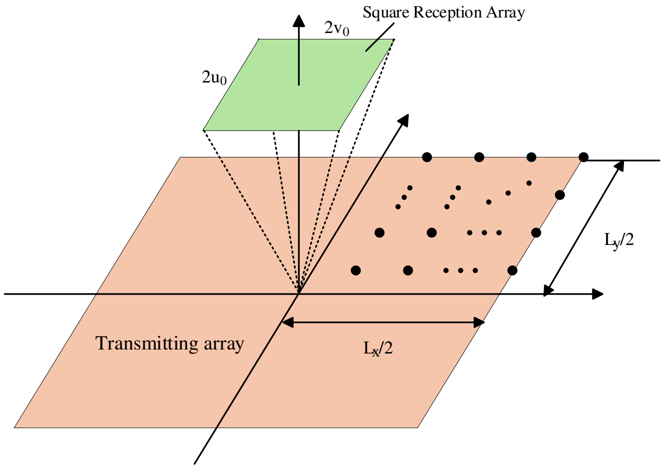

FIGURE 1. The model of the SDASPA.

array elements in the first quadrant only. The remaining three quadrants can be constructed by mapping the positions of the elements in the first quadrant using axial symmetry. In this model, it is assumed that the transmitting array is located on the XOY plane with an aperture size of $L_x \times L_y$. The array contains N elements, where the position coordinate of the n-th element is denoted as (x_n, y_n), and its corresponding excitation amplitude is I_n. The receiving array is located in the far-field region of the transmitting array. According to antenna theory, the array factor of the transmitting array can be expressed as:

$$F(u,v)=\sum_{n=1}^{N} I_n e^{jk(ux_n+vy_n)} \tag{1}$$

where $k = 2\pi/\lambda$ represents the wavenumber, and λ is the wavelength. $u = \sin\theta\cos\varphi$ and $v = \sin\theta\sin\varphi$ are the angular coordinates.

BCE is defined as the ratio of the power intercepted by the receiving area Ψ to the total power radiated over the entire visible region Ω. The receiving area Ψ is defined as $\{(u,v) : |u| \le u_0, |v| \le v_0\}$, and the visible region Ω is defined as $\{(u,v) : u^2+v^2 \le 1\}$. Therefore, the expression for BCE is:

$$\mathrm{BCE}=\frac{P_x}{P_a}=\frac{\int_{\Psi}|F(\theta,\varphi)|^2\,du\,dv}{\int_{\Omega}|F(\theta,\varphi)|^2\,du\,dv} \tag{2}$$

To facilitate computer optimization and solution, the integral form in the formula is transformed into a matrix operation form. Let the element excitation vector be $I = [I_1, I_2, \ldots, I_N]^T$ and the element direction vector be $V(u,v) = [e^{jk(ux_1+vy_1)}, \ldots, e^{jk(ux_N+vy_N)}]^T$. The array factor can be rewritten as $F(u,v) = I^T V(u,v)$. Thus, according to [10], BCE can be expressed as the ratio of two quadratic forms:

$$\mathrm{BCE}=\frac{\int_{\Psi} I^T V(u,v) I^H(u,v)\,du\,dv}{\int_{\Omega} I^T V(u,v) I^H(u,v)\,du\,dv}=\frac{I^H A I}{I^H C I} \tag{3}$$

where A and C are, respectively:

$$\begin{aligned} A &= \int_{\Psi} V(u,v) I^H(u,v)\,du\,dv, \\ C &= \int_{\Omega} V(u,v) I^H(u,v)\,du\,dv \end{aligned} \tag{4}$$

Additionally, CSL is an important indicator for measuring energy leakage, defined as the ratio of the maximum radiation intensity outside the receiving area to the maximum radiation intensity in the entire airspace, usually expressed in decibels (dB):

$$\mathrm{CSL(dB)}=10\lg\frac{\max\limits_{(\theta,\varphi)\notin\Psi}|F(\theta,\varphi)|^2}{\max\limits_{(\theta,\varphi)\in\Omega}|F(\theta,\varphi)|^2} \tag{5}$$

2.2. Subarray Division Model and Excitation Calculation

To reduce system complexity, this paper adopts subarray division technology. Assuming N array elements are divided into M subarrays ($M \ll N$), we define an $N \times M$ dimensional subarray division matrix:

$$SR=\begin{pmatrix} R_{11} & R_{12} & \ldots & R_{1M} \\ R_{21} & R_{22} & \ldots & R_{2M} \\ \vdots & \vdots & \ddots & \vdots \\ R_{N1} & R_{N2} & \ldots & R_{NM} \end{pmatrix} \tag{6}$$

The elements in the matrix are binary values (0 or 1):

$$R_{nm} = \begin{cases} 1, & \text{The } n\text{th element} \in \text{the } m\text{th subarray} \\ 0, & \text{else} \end{cases} \tag{7}$$

$$n = 1,2,\ldots,N; \quad m = 1,2,\ldots,M.$$

To ensure that each array element belongs to only one subarray and that there is no overlap, the following constraint must be satisfied:

$$\sum_{m=1}^{M} R_{nm} = 1, \quad \forall n \in \{1,2,\ldots,N\} \tag{8}$$

The specific method for subarray division is shown in Figure 2. In the proposed rule, the first-quadrant coordinates are compared with a set of lines having slope -1, and each threshold value b_m defines one boundary between adjacent subarrays. Because only the first-quadrant variables are optimized, the quantity $x_n + y_n$ is equivalent to the sum of the absolute values of the coordinates and can be used as a monotonic ordering variable for subarray assignment. Elements with smaller $x_n + y_n$ values are assigned to the inner regions, whereas elements with larger values are assigned to the outer regions. In this way, the aperture is partitioned into contiguous ring-like regions under axial symmetry, and all elements within the same

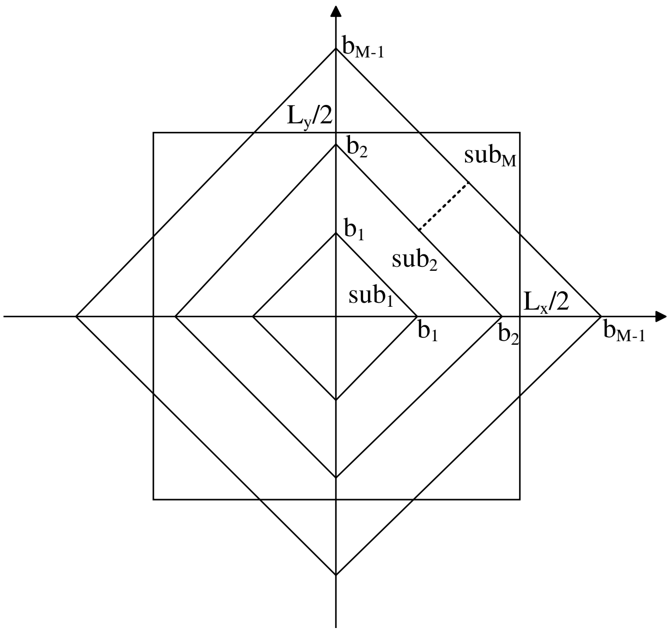

FIGURE 2. Subarray division model.

subarray share the same excitation amplitude, which can be illustrated as:

$$\begin{cases} \text{if } |x_n| + |y_n| < b_1, & R_{n1} = 1 \\ \text{else if } |x_n| + |y_n| < b_2, & R_{n2} = 1 \\ \quad \vdots & \\ \text{else if } |x_n| + |y_n| < b_{M-1}, & R_{nM-1} = 1 \\ \text{else}, & R_{nM} = 1 \end{cases} \tag{9}$$

$$n = 1, 2, \ldots, N$$

After dividing into M subarrays, all elements within the same subarray will share the same excitation amplitude. Define the subarray excitation vector as $W_{\text{sub}} = [w_1, w_2, \ldots, w_M]^T$. To maximize performance, the excitation value of each subarray is typically taken as the arithmetic mean of all original ideal excitations (optimal excitations before dividing) within that subarray. The calculation formula for the excitation w_m of the m-th subarray is:

$$w_m = \frac{\sum_{n=1}^{N} R_{nm} \cdot I_n^{\text{opt}}}{\sum_{n=1}^{N} R_{nm}} \tag{10}$$

Finally, the divided full-array excitation vector I_{final} can be obtained through the mapping of the division matrix:

$$I_{\text{final}} = SR \cdot W_{\text{sub}} \tag{11}$$

2.3. Description of the Optimization Model Based on SDASPA

To reduce the complexity of the feeding network while maintaining a high BCE, a one-step optimization framework is adopted for the SDASPA design. In the present work, BCE is treated as the primary objective while CSL is used as a performance indicator, and the number of subarrays M is fixed in each case to assess the trade-off between radiation performance and hardware complexity. The optimization variables therefore include the element coordinates and subarray boundary parameters. Owing to the axial symmetry of the array, only the variables in the first quadrant are updated during optimization, and the remaining elements are obtained by symmetry mapping. The optimization model can be formulated as:

$$\begin{cases} \text{find } [X, Y, B] = [x_1, x_2, \ldots, x_N, y_1, y_2, \ldots, \\ \qquad\qquad y_N, b_1, b_2, \ldots, b_{M-1}] \\ \text{maximize } \text{BCE}_{\max}[X, Y, B] \\ \text{subject to} \\ \text{(a)} \quad (x_{N/4}, y_{N/4}) = (L_x/2, L_y/2); \\ \text{(b)} \quad d_{\min}/2 \le x_n \le L_x/2,\ n = \left\{1, 2, \ldots, \frac{N}{4} - 1\right\}; \\ \text{(c)} \quad d_{\min}/2 \le y_n \le L_y/2,\ n = \left\{1, 2, \ldots, \frac{N}{4} - 1\right\}; \\ \text{(d)} \quad \sqrt{(x_i - x_j)^2 + (y_i - y_j)^2} \ge d_{\min}, \\ \qquad i, j \in \left\{1, 2, \ldots, \frac{N}{4}\right\}, i \ne j; \\ \text{(e)} \quad (x_n, y_n) = (-x_{n-N/4}, y_{n-N/4}), \\ \qquad n = \left\{\frac{N}{4} + 1, \ldots, \frac{N}{2}\right\}; \\ \text{(f)} \quad (x_n, y_n) = (-x_{n-N/2}, -y_{n-N/2}), \\ \qquad n = \left\{\frac{N}{2} + 1, \ldots, \frac{3N}{4}\right\}; \\ \text{(g)} \quad (x_n, y_n) = (x_{n-3N/4}, -y_{n-3N/4}), \\ \qquad n = \left\{\frac{3N}{4} + 1, \ldots, N\right\}; \\ \text{(h)} \quad d_{\min} < b_m < L_x - d_{\min},\ m = \{1, 2, \ldots, M-1\}; \\ \text{(i)} \quad b_m - b_{m-1} > 2d_{\min}, \quad m = \{1, 2, \ldots, M-1\}. \end{cases} \tag{12}$$

For clarity, the constraints in Equation (12) can be divided into four groups: aperture limits, minimum-spacing constraints, axial-symmetry constraints, and boundary-order constraints.

The objective of this model is to maximize BCE while satisfying physical constraints. Here, B denotes the set of subarray boundary parameters. The constraints in Equation (12) are enforced by a boundary-repair strategy: when a particle violates the feasible region, its coordinate or boundary value is projected back to the nearest valid boundary. In this way, the search space is restricted to physically realizable array configurations while the global exploration capability of particle swarm optimization (PSO) is preserved.

3. RT-DWCFPSO-SD ALGORITHM AND ITS APPLICATION FOR THE SYNTHESIS OF SDASPA

The RT-DWCFPSO-SD algorithm proposed in this paper is an improved PSO framework tailored to the SDASPA synthesis problem. A constriction factor, a dynamic inertia weight, and a ring topology are introduced to improve convergence stability and reduce the risk of premature convergence. In this implementation, the particle position encodes the element coordinates and subarray boundary parameters, and the fitness function is defined by the BCE value obtained after subarray division.

In the initial stage of iteration, a larger inertia weight facilitates the particles to search within the global range, avoiding premature convergence; in the later stage of iteration, a smaller weight facilitates fine searching within the local range. The dynamic weight formula adopted in this paper is as follows:

$$\omega = \omega_{\min} + (\omega_{\max} - \omega_{\min}) \times \left(1 - \frac{t}{T}\right)^2 \tag{13}$$

As the number of iterations increases, the inertia weight shows a nonlinear decreasing trend, which gives the algorithm a stronger late-stage search capability.

At the same time, the ring topology optimization method adopted in this paper is a common particle neighborhood structure in PSO. It arranges N particles in a circle, where each particle communicates only with its two adjacent neighbors (left and right), and optimization is guided by the neighborhood best particle [9], as shown in Figure 3. In contrast, the traditional optimization method is guided by the global best particle. Compared with the traditional method, although the ring topology method has a slower optimization speed, it maintains local information exchange, better preserves the diversity of the optimization algorithm, and reduces the risk of falling into local optima and converging prematurely in the early stages of the algorithm.

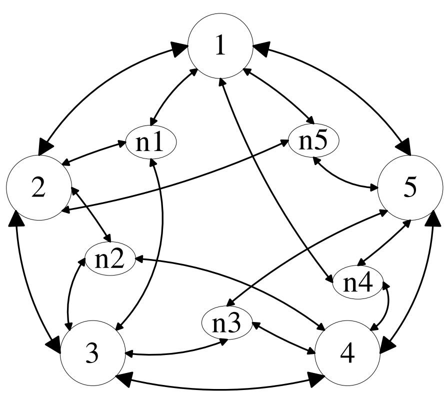

FIGURE 3. The model of ring topology.

The specific execution steps of the algorithm are as follows:

Step 1: Initialize parameters, including minimum element space $d_{\min}$, array aperture $L_x \times L_y$, number of elements $N = 4 \times N_x \times N_y$, number of subarrays M, population size NP, maximum number of iterations T, cognitive and social acceleration coefficients c_1, c_2, upper and lower limits of inertia weight $\omega_{\max}$, $\omega_{\min}$, etc. Randomly initialize the position (x_n, y_n) and velocity v_n of the array elements represented by each particle, as well as the subarray division parameter b_m and its velocity v_b.

Step 2: Divide the subarrays according to the method in Equation (9) to obtain the subarray division matrix. Calculate the element excitation vector I_{opt} for each particle according to Equation (3). Sequentially, calculate the final element excitation amplitude of each particle after subarray division according to Equations (10) and (11). Calculate the BCE value for each particle after subarray division according to Equation (2), and record the best BCE value as personal best solution ($pbest$). Then, select the best BCE out of the three neighboring particles as neighborhood best solution ($lbest$).

Step 3: Update the velocity and position of the array element represented by each particle according to the following formula. To balance global exploration and local exploitation capabilities, a constriction factor χ and dynamic inertia weight ω are introduced:

$$\begin{aligned} \nu_{x_{t+1}} &= \chi \times [\omega \times \nu_{x_t} + c_1 \times rand \times (pbest_{x_t} - x_t) \\ &\quad + c_2 \times rand \times (lbest_{x_t} - x_t)] \\ x_{t+1} &= x_t + \nu_{x_{t+1}} \end{aligned} \tag{14}$$

where t is the current iteration number; $rand$ are random numbers between $[0, 1]$; the constriction factor χ is:

$$\begin{cases} \phi = c_1 + c_2 \\ \chi = \dfrac{2}{\left|2 - \phi - \sqrt{\phi^2 - 4\phi}\right|} \end{cases} \tag{15}$$

Step 4: Update the subarray division parameters represented by each particle according to the following formula, and the principle is the same as Step 3:

$$\begin{aligned} \nu_{b_{t+1}} &= \chi \times [\omega \times \nu_{b_t} + c_1 \times rand \times (pbest_{b_t} - b_t) \\ &\quad + c_2 \times rand \times (lbest_{b_t} - b_t)] \\ b_{t+1} &= b_t + \nu_{b_{t+1}} \end{aligned} \tag{16}$$

Step 5: Check whether the updated element coordinates or boundary parameters violate the aperture range, minimum-spacing constraint, or the ordering of the subarray boundaries. If a violation occurs, repair the infeasible particle by projecting it back to the feasible domain.

Step 6: Determine whether the maximum number of iterations T has been reached. If yes, terminate the search and select the best $pbest$ as $gbest$; otherwise, return to Step 2 and continue iterating.

Step 7: Output the optimal subarray division matrix SR, the optimal subarray excitation vector W_{sub}, the best solution $gbest$, and the corresponding array layout. Then compute the CSL for the final design.

The pseudo-code flow of the algorithm is shown in Figure 4.

4. SIMULATION RESULTS AND ANALYSIS

To verify the effectiveness of the SDASPA and RT-DWCFPSO-SD proposed in this paper, this section presents a detailed analysis via numerical simulation. First, we use the RT-DWCFPSO-SD algorithm to optimize the SDASPA model to verify the validity of the proposed method. Next, to demonstrate the superiority of the proposed model, we use RT-DWCFPSO-SD to optimize the nonuniform distributed planar array (NDPA) and the nonuniform distributed sparse planar array (NDSPA), respectively, under invariant parameters, and compare the optimization results of these three models with array models from the literature. Finally, to illustrate the superiority of the RT-DWCFPSO-SD algorithm compared to other algorithms, its optimization results are compared with those of four other PSO algorithms under the same parameter conditions.

The pseudo-code of the RT-DWCFPSO-SD algorithm

Initialize parameters.
For t = 1 : T
  For *NP_count* = 1 : *NP*
    Generate subarray division matrix *SR* according to (9).
    Calculate I_{opt} according to (3).
    Calculate W_{sub} and I_{final} according to (10) and (11).
    Calculate *BCE* according to (2) and update *pbest* and *lbest*.
    Update the position of array elements according to (14).
    Update the subarray division parameters according to (16).
    Constraint the particles out of boundary to the boundary.
  End
End
Select the best *pbest* as *gbest*.
Output crucial data after optimization and calculate *CSL*.

FIGURE 4. Pseudo-code flow of the RT-DWCFPSO-SD algorithm.

The parameter conditions related to RT-DWCFPSO-SD include: wavelength $\lambda = 1$, array aperture $L_x \times L_y = 4.5\lambda \times 4.5\lambda$, number of elements $N = 8 \times 8$, receiving area range $u_0 = v_0 = 0.2$, number of particles $NP = 50$, and maximum number of iterations $T = 200$. All simulation experiments in this paper were completed on the same computing platform: the hardware platform is AMD Ryzen 7-7735H, with a main frequency of 3.2 GHz and a memory size of 16 GB, and the simulation software is MATLAB R2024b.

4.1. Optimization Results of RT-DWCFPSO-SD Algorithm on SDASPA Model

This section utilizes the proposed RT-DWCFPSO-SD algorithm to optimize the SDASPA model. This model adopts a sparse distribution strategy with a minimum element space of $d_{\text{min}} = 0.6$. We tested scenarios where the array is divided into 2, 3, and 4 subarrays. The optimization results are shown in Table 1.

TABLE 1. Optimizing results of SDASPA using RT-DWCFPSO-SD algorithm.

M	W_{sub}	BCE (%)	CSL (dB)
2	0.8715, 0.3258	90.73	−14.08
3	0.8617, 0.3912, 0.1595	93.42	−13.19
4	1.0000, 0.8417, 0.3843, 0.1618	93.82	−12.63

As shown in Table 1, increasing the number of subarrays provides more design freedom and improves BCE. In the tested cases, the 4-subarray configuration achieves the highest BCE, whereas the 3-subarray configuration provides a slightly lower BCE but a better balance between BCE, CSL, and implementation complexity. Considering that the 3-subarray case requires only three power amplifiers and still maintains a low sidelobe level, it is selected as the preferred compromise for the present design scenario. The simulation figures further show that the majority of the radiated power is concentrated within the receiving area, confirming the beam-collection capability of the proposed method.

To visually display the optimization effect, Figures 5, 6, and 7 show the element position excitation plots and normalized power patterns, when the number of subarrays is 2, 3, and 4, respectively. In the element position excitation plots, different colors represent different subarrays, and the size or color depth of the points represents the excitation amplitude. The normalized power patterns show that most of the energy is concentrated in the central receiving area, and the sidelobe levels are effectively suppressed, verifying the excellent beam-collection performance of the proposed method.

4.2. Comprehensive Comparison with Existing Array Models

To further illustrate the superiority of the SDASPA model proposed in this paper, we used the same RT-DWCFPSO-SD algorithm to optimize the NDPA model and NDSPA model. The optimization results are shown in Figures 8 and 9, when the number of subarrays is 3.

Furthermore, we comprehensively compared the optimization results of above three models with the models in [10–12]. The comparison indicators include the number of elements N, number of subarrays M, BCE, CSL, amplifier sparsity $\gamma_a \triangleq M/N$, and element sparsity $\gamma_e \triangleq N/N_{\text{full}}$ (where N_{full} represents the number of elements in a full array). The comparison results are shown in Table 2.

Table 2 provides a preliminary comparison between the proposed SDASPA model and the reference models reported in [10–12]. Because the compared cases do not share the same

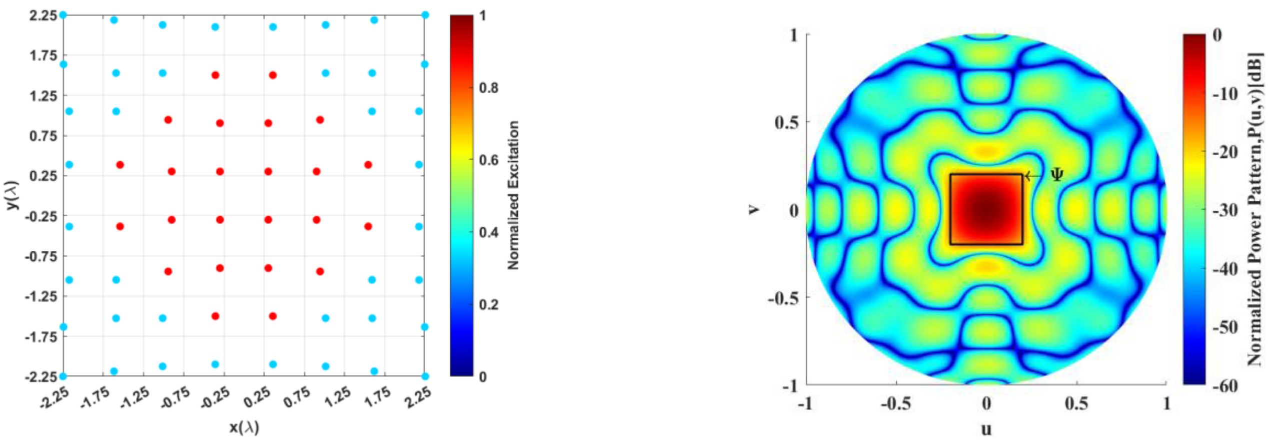

FIGURE 5. Simulation results of SDASPA model when $M = 2$.

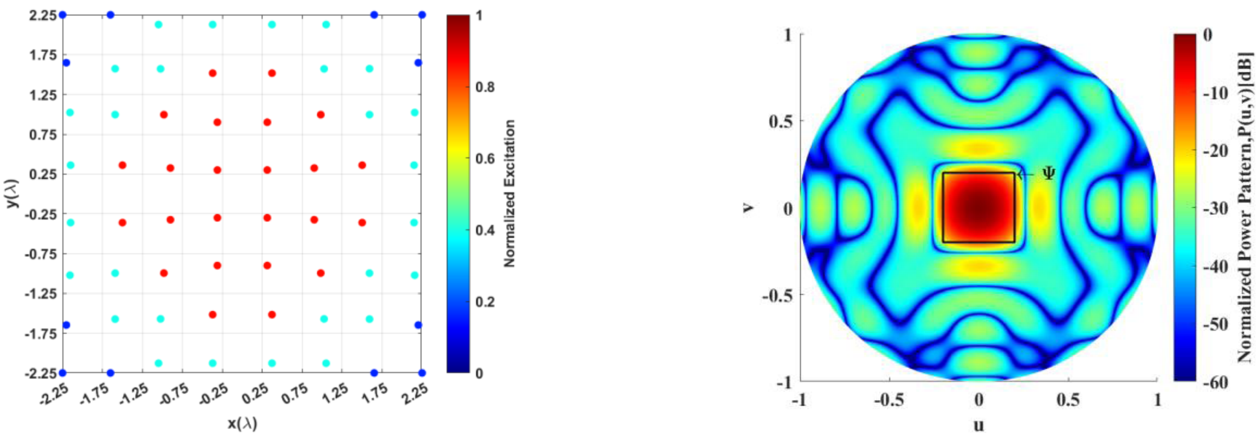

FIGURE 6. Simulation results of SDASPA model when $M = 3$.

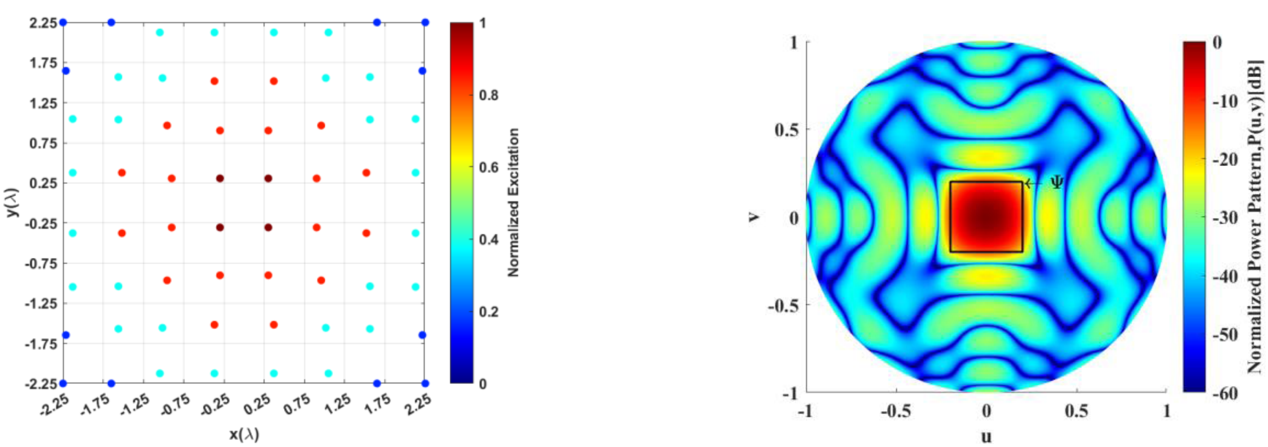

FIGURE 7. Simulation results of SDASPA model when $M = 4$.

aperture, element count, and modeling assumptions, the numerical comparison should be interpreted with caution. Under the conditions reported here, the proposed SDASPA case achieves a favorable trade-off between BCE and CSL while retaining a low subarray count. This comparison indicates that the axial-symmetry strategy and sparse-structure design are effective for MWPT transmitting arrays, but a fully controlled benchmark study under matched conditions is still desirable.

4.3. Comparison with Other PSO Algorithms

To verify the superiority of the proposed algorithm in optimization capability, we compared RT-DWCFPSO-SD algorithm with standard PSO (SPSO) [13], constriction factor PSO (CFPSO) [7], and nonlinear dynamic weight PSO (NDWPSO) [14] under the same conditions. The simulation was performed on the SDASPA model ($M = 3$, $d_{\min} = 0.6$). The comparison results are shown in Table 3.

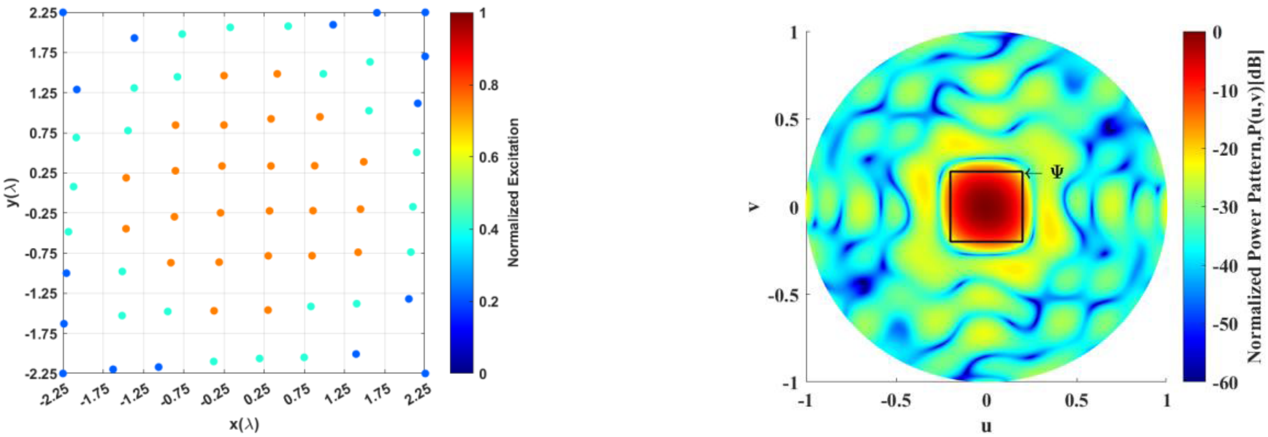

FIGURE 8. Simulation results of NDPA model when $M = 3$.

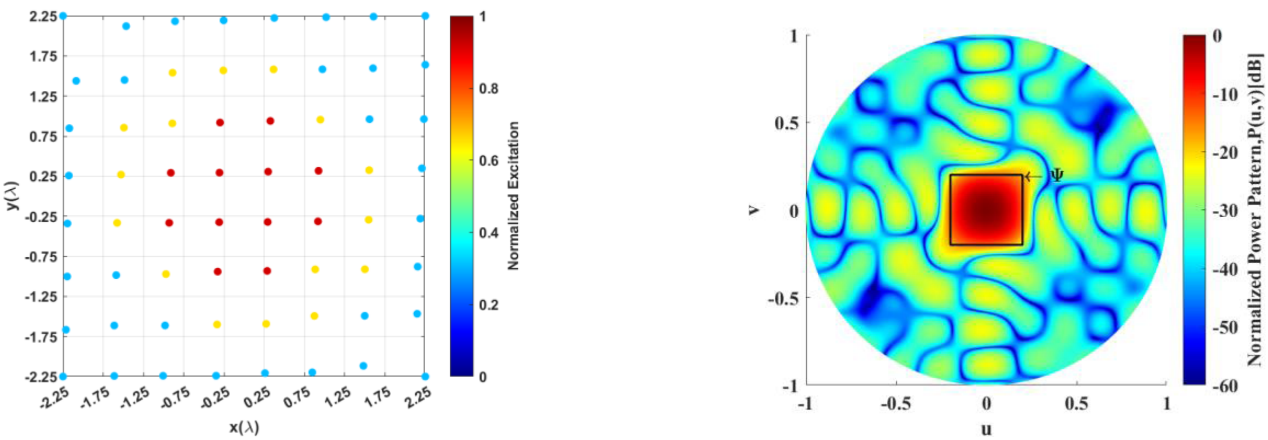

FIGURE 9. Simulation results of NDSPA model when $M = 3$.

TABLE 2. Comparison results of various array models.

	SDASPA	NDPA	NDSPA	Ref. [10]	Ref. [11]	Ref. [12]
N	64	64	64	100	100	64
M	3	3	3	1	1	3
BCE (%)	93.42	89.80	90.68	86.48	91.06	91.37
CSL (dB)	-13.19	-11.77	-13.31	-7.78	-16.01	-17.64
γ_a (%)	4.6875	4.6875	4.6875	1	1	4.6875
γ_e (%)	64	64	64	100	100	64

TABLE 3. Comparison of simulation results of various PSO algorithms.

BCE(%)				
Algorithm	Maximum Value	Minimum Value	Average Value	Standard Deviation
SPSO	92.67	91.78	92.10	1.92×10^{-3}
CFPSO	92.92	92.32	92.64	1.36×10^{-3}
NDWPSO	93.13	92.66	92.87	1.22×10^{-3}
RT-DWCFPSO-SD	93.64	93.18	93.42	1.05×10^{-3}

Table 3 compares the proposed RT-DWCFPSO-SD algorithm with SPSO, CFPSO, and NDWPSO under the same simulation settings. The results show that the proposed algorithm converges more slowly than some of the baseline methods in the early iterations, but it maintains better population diversity and is less prone to premature convergence. As a result, it reaches a more competitive final solution in the tested cases. These observations indicate that the combined use of ring topology, constriction factor, and dynamic inertia weight is beneficial for the present sparse subarray-division problem.

5. CONCLUSION

In this paper, an SDASPA model and an RT-DWCFPSO-SD algorithm are proposed for MWPT transmitting-array synthesis under limited subarray divisions. The proposed framework performs one-step joint optimization of the element coordinates, element excitations, and subarray boundary parameters, with BCE as the primary objective. Numerical simulations show that, for the tested 8×8 array with a $4.5\lambda \times 4.5\lambda$ aperture, dividing the array into three subarrays can achieve a BCE of 93.42% while maintaining a CSL of -13.19 dB. These results suggest that the proposed method is a useful theoretical design tool for sparse MWPT arrays. Future work will focus on repeated-run statistical validation, matched-condition benchmarking, and hardware-level experimental verification.

REFERENCES

[1] Xiao, D., L. Tian, L. Xu, H. Zhang, and X. Wang, "Fast beam-pointing control algorithms based on deep learning models for moving target in MWPT," *IEEE Transactions on Antennas and Propagation*, Vol. 72, No. 5, 4541–4548, 2024.

[2] Yazdandoost, K. Y. and R. Kohno, "Wireless communications for body implanted medical device," in *2007 Asia-Pacific Microwave Conference*, 1–4, Bangkok, Thailand, 2007.

[3] Ma, H., Y. Yang, N. Qi, S. Ma, and X. Li, "Demonstration of a high-efficiency MWPT system for aerospace," in *2018 IEEE Wireless Power Transfer Conference (WPTC)*, 1–4, Montreal, QC, Canada, 2018.

[4] Jiang, H. and W. Dou, "Methods for improving the distance of microwave wireless power transmission with a given beam collection efficiency," *IEEE Antennas and Wireless Propagation Letters*, Vol. 19, No. 12, 2112–2116, 2020.

[5] Massa, A., G. Oliveri, F. Viani, and P. Rocca, "Array designs for long-distance wireless power transmission: State-of-the-art and innovative solutions," *Proceedings of the IEEE*, Vol. 101, No. 6, 1464–1481, 2013.

[6] Yao, Y., L. W. Song, and Y. L. Liu, "Subarray partition design of receiving antenna for microwave power transmission," in *2019 International Conference on Microwave and Millimeter Wave Technology (ICMMT)*, 1–3, Guangzhou, China, 2019.

[7] Clerc, M. and J. Kennedy, "The particle swarm-explosion, stability, and convergence in a multidimensional complex space," *IEEE Transactions on Evolutionary Computation*, Vol. 6, No. 1, 58–73, 2002.

[8] Na, L., J. Yan, and L. Shu, "Application of PSO algorithm with dynamic inertia weight in medical image thresholding segmentation," in *2017 IEEE 19th International Conference on e-Health Networking, Applications and Services (Healthcom)*, 1–4, Dalian, China, 2017.

[9] Li, X., "Niching without niching parameters: Particle swarm optimization using a ring topology," *IEEE Transactions on Evolutionary Computation*, Vol. 14, No. 1, 150–169, 2010.

[10] Oliveri, G., L. Poli, and A. Massa, "Maximum efficiency beam synthesis of radiating planar arrays for wireless power transmission," *IEEE Transactions on Antennas and Propagation*, Vol. 61, No. 5, 2490–2499, 2013.

[11] Li, X., B. Duan, J. Zhou, L. Song, and Y. Zhang, "Planar array synthesis for optimal microwave power transmission with multiple constraints," *IEEE Antennas and Wireless Propagation Letters*, Vol. 16, 70–73, 2017.

[12] Li, J., Z. Han, and C. Guo, "Novel subarray partition algorithm for solving the problem of too low beam collection efficiency caused by dividing a few subarrays," *Progress In Electromagnetics Research M*, Vol. 108, 223–235, 2022.

[13] Miao, A.-M., X.-L. Shi, J.-H. Zhang, E.-Y. Wang, and S.-Q. Peng, "A modified particle swarm optimizer with dynamical inertia weight," in *Fuzzy Information and Engineering Volume 2*, Vol. 62, 767–776, Berlin, Heidelberg, 2009.

[14] Liu, Y., J. Xi, H. Bai, Z. Wang, and L. Sun, "A general robot inverse kinematics solution method based on improved PSO algorithm," *IEEE Access*, Vol. 9, 32 341–32 350, 2021.